Preparation and structural characterization of ferromagnetic $Mn_5Si_3C_x$ films

C. Sürgers,[1] M. Gajdzik,[1] G. Fischer,[1] H. v. Löhneysen,[1,2] E. Welter,[3] and K. Attenkofer[3,*]
[1]*Physikalisches Institut, Universität Karlsruhe, D-76128 Karlsruhe, Germany*
[2]*Forschungszentrum Karlsruhe, Institut für Festkörperphysik, D-76021 Karlsruhe, Germany*
[3]*Hamburger Synchrotronstrahlungslabor (HASYLAB), am Deutschen Elektronensynchrotron (DESY), Notkestrasse 85, D-22603 Hamburg, Germany*

(Received 15 July 2003; revised manuscript received 11 September 2003; published 19 November 2003)

Carbon-doped Mn-Si films prepared by magnetron sputtering at elevated substrate temperatures exhibit ferromagnetic order for compositions around $Mn_5Si_3C_x$ ($x>0$) in contrast to the antiferromagnetic Mn_5Si_3 compound. In these sputtered samples the carbon concentration can be strongly enhanced compared to sintered powder samples. The local structural order around the Mn site in $Mn_5Si_3C_x$ films was investigated for $x=0$ and 0.75 by x-ray-absorption spectroscopy at different temperatures T. At low T, both films retain their hexagonal structure and do not exhibit the orthorhombic distortion observed for bulk Mn_5Si_3 powder. For the carbon-doped film a local distortion of the octahedra formed by six Mn atoms of the Mn_5Si_3 structure is found when surrounding a C atom. This indicates an anisotropic change of the atomic Mn environment by C, in contrast to a simple lattice expansion as inferred from previous structural analysis.

DOI: 10.1103/PhysRevB.68.174423 PACS number(s): 75.70.−i, 74.62.Dh, 81.15.−z

I. INTRODUCTION

Manganese compounds exhibit a number of properties which are of fundamental and/or technological interest, such as the quantum-critical behavior of MnSi (Ref. 1) or the colossal magnetoresistance of $La_{1-x}Sr_xMnO_3$.[2] Although many intermetallic compounds of Mn and Si or Ge exhibit antiferromagnetic or ferrimagnetic order, it has been shown earlier that carbon-doped $Mn_5Si_3C_x$ shows ferromagnetic behavior with a maximum Curie temperature $T_C=152$ K for $x=0.22$ in contrast to antiferromagnetic Mn_5Si_3.[3] The unit cell of the hexagonal Mn_5Si_3 structure (space group $P6_3/mcm$) contains four Mn_I atoms at position $4(d)$ (1/3,2/3,0), six Mn_{II} atoms at position $6(g)$ (y_{Mn},0,1/4) with $y_{Mn}=0.2358$, and six Si atoms at position $6(g)$ (y_{Si},0,1/4) with $y_{Si}=0.5991$.[3,4] For the carbon-doped samples previous structural analysis suggests that the carbon is incorporated into the interstitial voids at position $2(b)$ (0,0,0) of the Mn_{II} octahedra up to a C concentration $x\approx0.22$.[3] Such phases with filled $D8_8$ structure are usually denoted as ''Nowotny phases.''[3,5,6] The binding of impurity atoms such as C, N, and O into the octahedral cavities of the Mn_5Si_3-type structure has been established for several different compounds and is still a topic of recent research in physical chemistry.[6]

However, the magnetic properties of such carbon-doped compounds have not been widely studied so far. In this respect it is remarkable that the saturation of carbon uptake in $Mn_5Si_3C_x$ can be enhanced up to $x\approx1$ by magnetron sputtering of films from elemental targets.[7] The magnetic properties of these films have been investigated previously by the magneto-optic Kerr effect and magnetometry.[7,8] A maximum $T_C=350$ K was obtained for a substrate temperature $T_S=470\,^\circ$C. The enhancement of T_C by carbon doping was also demonstrated for isostructural Mn_5Ge_3 films.[9] Because of the complication of structurally inequivalent Mn sites with different Mn neighbor arrangements, different local magnetic moments were deduced from broadband nuclear-magnetic-resonance measurements and band-structure calculations.[10,11] Furthermore, the appearance of ferromagnetic hysteresis curves at temperatures well above room temperature was reported for annealed Mn/C/Si triple layers[12] and C/Mn/C/Si multilayers.[13] However, in these samples the crystallographic structure of the ferromagnetic phase is unclear.

In this paper we will focus on the preparation and structural properties of Mn-Si-C films deposited by magnetron sputtering with various C concentrations. In this respect the magnetic data such as T_C and the average magnetic moment per Mn atom reported earlier will only serve as parameters characterizing the magnetic properties. We demonstrate that the $Mn_5Si_3C_x$ phase is formed in a restricted range of substrate temperatures and that films with a composition around $Mn_5Si_3C_{0.75}$ exhibit the highest Curie temperature. This suggests that this phase is likely to occur also in the aforementioned annealed Mn/C/Si triple layers and C/Mn/C/Si multilayers. In addition, the local atomic structure around the Mn site was studied by x-ray-absorption spectroscopy (XAS) at the Mn K edge to obtain further information of the effect of carbon doping on the Mn valency and on the local atomic Mn environment.

II. EXPERIMENT

Mn-Si-C films were prepared by simultaneous dc- and rf-magnetron sputtering from elemental targets of Mn (99.99% purity), Si (99.999% purity), and C (99.9% purity) in a high-vacuum system (base pressure 5×10^{-7} mbar) under argon atmosphere ($p_{Ar}=5\times10^{-3}$ mbar) on single-crystalline Si (001) or Al_2O_3 ($1\bar{1}02$) substrates at different substrate temperatures T_S. The typical film thickness was 100 nm except for XAS, where films of 220 nm thickness were measured. In addition, a Mn_5Si_3 powder sample was prepared for comparison with the XAS data of the films. This sample was obtained by annealing a pellet of mixed powder in a quartz tube under argon atmosphere for 184 h at 900 °C.[14] The reacted Mn_5Si_3 powder was finally pressed to

a pellet together with polyethylene powder. Film homogeneity, i.e., the composition profile along the growth direction, was checked by means of Auger sputter depth profiling in a separate ultrahigh vacuum system.[15] For this purpose, the film was sputter etched by a focused 1-keV Ar^+ ion beam of 3 mm diameter. During sputtering, Auger spectra were continuously recorded using a 3-keV electron beam of ≈ 0.1 mm diameter for excitation. Concentration profiles were obtained by plotting the respective Auger peak-to-peak heights (dN/dE) of Mn (589 eV), Si (92 eV), and C (272 eV) vs sputtering time, i.e., vs sputter etched depth.

The samples were magnetically characterized by means of the transverse magneto-optical Kerr effect for temperatures $T=2$–400 K as described earlier.[7,8] The Curie temperature was determined from an extrapolation of the magnetization $M(T)$ to $M(T_C)=0$ measured in a weak magnetic field of 5 mT.

X-ray diffraction was done with Cu K_α radiation in a $\theta/2\theta$ powder diffractometer with Bragg-Brentano focusing, which only provides information about the lattice plane distances along the normal of the film, i.e., along the growth direction. Some films have also been measured at $T=25$ K using a liquid-He flow cryostat.

XAS data at the Mn K edge were taken in fluorescence mode at HASYLAB, beam line A1. The synchrotron radiation was monochromatized using two channel-cut Si (111) crystals operated either in the four-crystal mode for high resolution in the near-edge region ($\Delta E=0.5$ eV) or in the two-crystal mode in the extended XAS region beyond the absorption edge ($\Delta E=1.5$ eV). The monochromator was slightly detuned to 70% or 50% maximum intensity, respectively, to reject higher harmonic reflections. Mn fluorescence radiation was measured with a Ge detector oriented at angles of 90° and 45° with respect to the incoming beam and the sample surface, respectively. Background radiation, in particular Fe fluorescence, was minimized by electronic discrimination. Sample cooling was obtanined by a liquid-He flow cryostat operating at temperatures 5–300 K. XAS was done in two different energy regimes, i.e., in the near-edge region to provide information about the influence of carbon on the Mn valence state and in the region of extended x-ray-absorption fine structure (EXAFS) to investigate the local atomic order around the Mn atoms. The energy scale of every spectrum was calibrated by the spectrum of an α-Mn foil measured simultaneously, with a K edge at $E_K=6537.7$ eV as determined from the inflection point (root of second derivative). Further XAS data analysis was done by means of the computer program WINXAS.[16]

III. RESULTS AND DISCUSSION

A. Film preparation

Previous investigations on vapor deposited Mn-Si-C films of unknown composition have shown that the occurrence of magnetic hysteresis curves above room temperature is correlated with the presence of the Mn_5Si_3 phase.[8] Therefore, Mn-Si-C films with various compositions around the stoichiometric Mn_5Si_3 compound were prepared at $T_S=470$ °C. This substrate temperature was found to be optimum for the formation of a nearly single-phase material, see below. Figure 1 shows the Curie temperature for a number of Mn-Si-C films with different compositions. Obviously, the highest T_C values are obtained for compositions along the $Mn_5Si_3C_x$ line. In particular, samples with $x=0.75$ have $T_C=352$ K and a maximum average magnetic moment of 1 μ_B/Mn atom.[7] This indicates that the $Mn_5Si_3C_{0.75}$ films are the most stable ones in terms of magnetic order. The electrical resistance ρ of these films shows a linear temperature dependence above ≈ 50 K with $\partial\rho/\partial T>0$ characteristic for metallic behavior with, however, a high residual resistivity $\rho_0=250$ $\mu\Omega$ cm and a resistance ratio $R_{300\,K}/R_{10\,K}=1.8$, see Fig. 2. Films with $x>1$ have a much larger resistivity presumably due to the larger number of defects caused by a doping level much higher than the optimum doping level. In addition, they exhibit a minimum around 40 K and an upturn in resistivity towards lower temperatures, characteristic for strongly disordered metals such as metallic glasses.

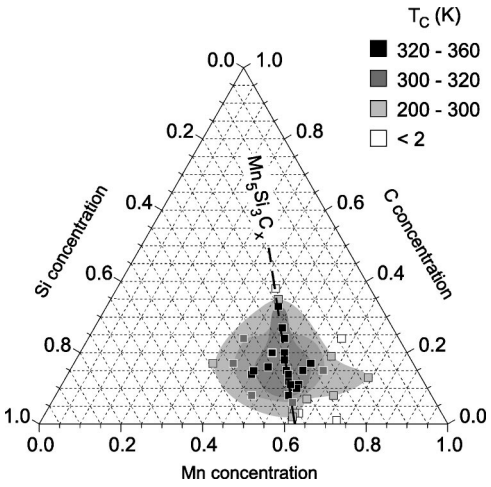

FIG. 1. Curie temperature of Mn-Si-C alloy films in dependence of the concentration in atomic percent. Gray scale indicates the magnitude of T_C. Dashed line marks the composition of $Mn_5Si_3C_x$.

In order to gain more information on alloy formation, the role of the substrate material was also studied. Figure 3 shows the Curie temperature vs T_S for films with $x=1.5$ deposited on Si (001) or Al_2O_3 ($1\bar{1}02$) substrates. From this plot an optimum $T_S=470$ °C is obtained where T_C is maximum. Films deposited at higher T_S have a higher T_C when

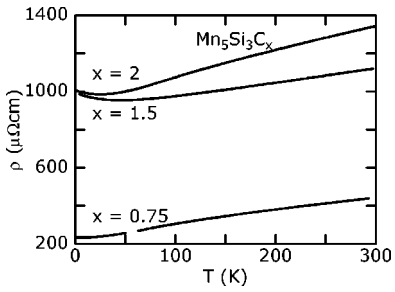

FIG. 2. Resistivity ρ vs temperature T for $Mn_5Si_3C_x$ films with different composition x, sputtered at $T_S=470$ °C.

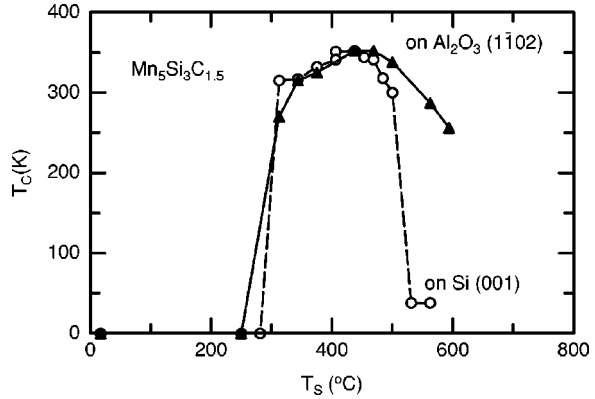

FIG. 3. Curie temperature T_C of $Mn_5Si_3C_{1.5}$ films deposited on Si (circles) or sapphire (triangles) at different substrate temperatures T_S.

sputtered on sapphire compared to films sputtered on silicon substrates, whereas for $T_S \leqslant 470°C$ the type of substrate seems to be irrelevant. The precipitous drop of T_C for films deposited on Si (001) is due to a strong interdiffusion between film and substrate. This can be inferred from the Auger depth profiles of Mn, Si, and C shown in Fig. 4 for films prepared at $T_S = 470\,°C$. Note that the nominal Mn/Si ratio given by the sputtering rates is the same for all films. For $x = 1.5$, the film is only slightly enriched with Si as deduced

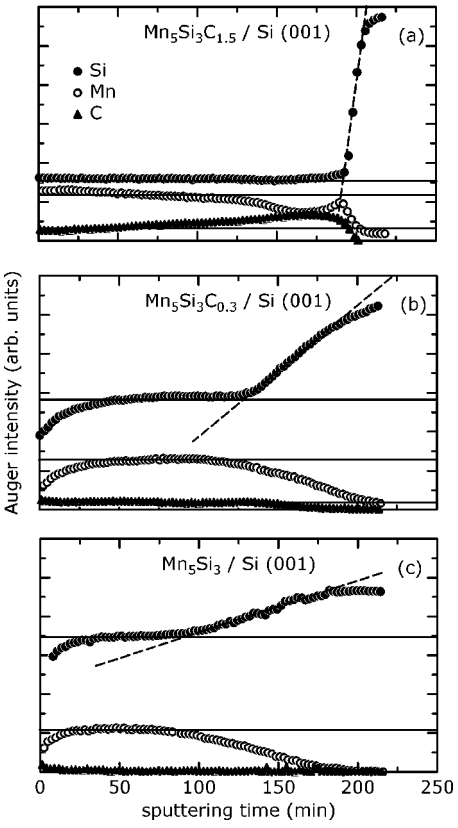

FIG. 4. Auger depth profiles of films with nominal $Mn_5Si_3C_x$ composition deposited on Si (001) substrates at $T_S = 470\,°C$. Solid lines mark the average concentration in the film. Dashed lines indicate the region of strong interdiffusion between film and substrate.

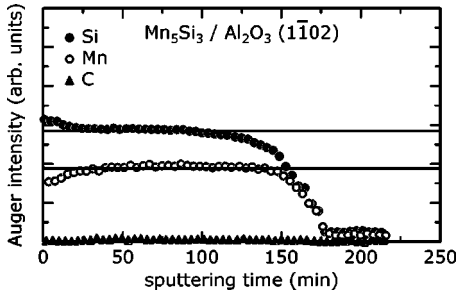

FIG. 5. Auger depth profile of a Mn_5Si_3 film deposited on a $(1\bar{1}02)$ sapphire substrate at $T_S = 470\,°C$.

from the composition ratio Mn:Si:C = 47:38:15 (at. %) estimated from the averaged Auger intensities by taking elemental Auger sensitivity factors into account, which differs only slightly from the nominal deposited composition 53:32:15. However, films with a smaller carbon content are severely enriched with silicon. In addition, a Mn depleted interface region of almost half the film thickness is formed. The fact that the width of this interface decreases with increasing x indicates that the $Mn_5Si_3C_x$ alloy formed at elevated temperatures is more stable with a lower Gibbs free energy of formation compared to the parent Mn_5Si_3 compound. This could be due to a larger contribution of reaction entropy for the carbon-doped sample. The interdiffusion is not observed for Mn_5Si_3 films deposited on sapphire substrates. These latter samples show a constant concentration over the whole film thickness and an instant decrease of the Si and Mn signal when the film/substrate boundary is reached, see Fig. 5. Hence, all films discussed in the following were deposited on sapphire $(1\bar{1}02)$ substrates.

B. X-ray diffraction

Figure 6(a) shows x-ray diffractograms for films deposited at different T_S. At $T_S = 470\,°C$ the main characteristic reflections of the Mn_5Si_3 structure are observed. Minor Bragg reflections are not seen due to the small amount of polycrystalline material. However, an earlier high-resolution x-ray-diffraction study on a $Mn_5Si_3C_{1.5}$ powder sample (obtained by sputtering several 1000-nm thick films on NaCl substrates which were subsequently dissolved in water) exhibited the whole set of Bragg reflections expected for the Mn_5Si_3 structure.[7] The differences in the relative height of the reflections compared to the data of the randomly oriented Mn_5Si_3 powder indicate a prominent texture of the sputtered films along the growth direction, which is preferentially the hexagonal c axis. In Fig. 6(a) the diffractogram of a film deposited at lower T_S shows only a strongly broadened maximum around $2\theta = 43°$, characteristic for the existence of an amorphous phase. At $T_S = 570\,°C$, i.e., much higher than the optimum T_S, crystallographic phases other than Mn_5Si_3 are formed. For this sample the Curie temperature is already reduced to below room temperature, see Fig. 3.

The effect of carbon concentration x on the structure of $Mn_5Si_3C_x$ films deposited at $T_S = 470\,°C$ is shown in Fig. 6(b). For $x = 0$, a strong texture is observed as already men-

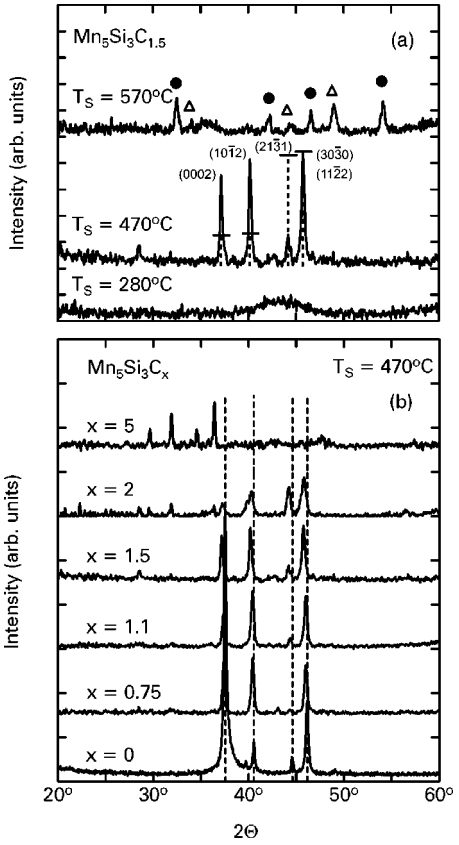

FIG. 6. $\theta/2\theta$ x-ray diffractograms for (a) $Mn_5Si_3C_{1.5}$ films prepared at different T_S and (b) $Mn_5Si_3C_x$ films prepared at $T_S = 470\,^{\circ}C$. Symbols indicate reflections due to $Mn_{27}Si_{47}$ (closed circles) and MnSi (open triangles). Dashed lines indicate reflections due to the $Mn_5Si_3C_x$ Nowotny phase. Horizontal bars in (a) mark the intensities expected for a random oriented powder sample.

tioned, which decreases with increasing x as can be seen from the relative intensity of the (0002) reflection. The data clearly show that the Mn_5Si_3 structure is stable up to $x = 1.1$. The reflections shift to lower angles indicating an increase of the lattice parameters with increasing x.

The unit-cell volume estimated from the lattice constants is plotted in Fig. 7 vs concentration x for films sputtered at $T_S = 470\,^{\circ}C$. The lattice constants were obtained by a least-squares fit of the Mn_5Si_3 structure to the measured lattice-plane distances: $a = 6.907$ Å, $c = 4.800$ Å for Mn_5Si_3; $a = 6.939$ Å, $c = 4.831$ Å for $Mn_5Si_3C_{0.75}$. Also shown are data obtained from earlier measurements on sintered $Mn_5Si_3C_x$ powder samples.[3] The unit-cell volume of the films increases roughly linearly up to $x = 1$ and eventually saturates in contrast to the sintered powder samples, which exhibit a saturation of the unit-cell volume already at $x = 0.22$. Presumably, for films with $x \approx 1$ all octahedral voids are filled by carbon atoms leading to a saturation.

Figure 6(b) shows that for $x \geqslant 1.5$ the amount of the Mn_5Si_3 phase decreases as inferred from the gradual disappearance of the Mn_5Si_3 reflections and the appearance of additional reflections originating from other crystalline phases, for instance, pure Mn, SiC, and Mn_8Si_2C. This is in agreement with the concentration dependence of the magnetic moment μ/Mn-atom which strongly decreases for $x > 1$ with increasing x.[7] Therefore, from x-ray-diffraction analysis $T_S = 470\,^{\circ}C$ and a carbon content of $0 \leqslant x \leqslant 1$ are found as optimum preparation parameters for the formation of nearly single-phase $Mn_5Si_3C_x$ films. In particular, $Mn_5Si_3C_{0.75}$ films are the most stable ones in terms of magnetic order.

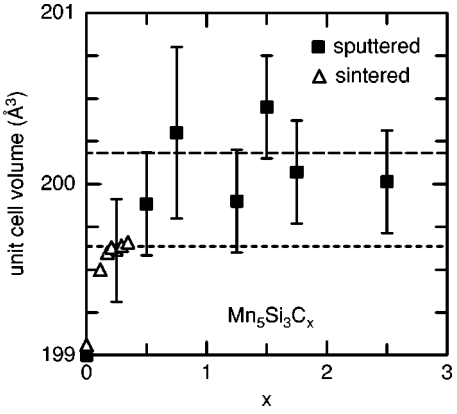

FIG. 7. Unit-cell volume vs carbon concentration x of sputtered $Mn_5Si_3C_x$ films (solid squares) and sintered $Mn_5Si_3C_x$ powder samples after Ref. 3 (open triangles). Dashed lines indicate the respective saturation values.

C. X-ray-absorption spectroscopy

Figure 8 shows the x-ray absorption, i.e., fluorescence yield, normalized to the intensity well above the discontinuity vs photon energy E. The preedge at a, originating from electronic transitions from the $1s$ core level into the d states of the conduction band, is preserved for all samples in agreement with previous near-edge data of several Mn compounds.[17] Although these transitions are forbidden by dipole selection rules, the states are accessible due to s-p-d hybridization. A mixing of the of p-like and d-like states was

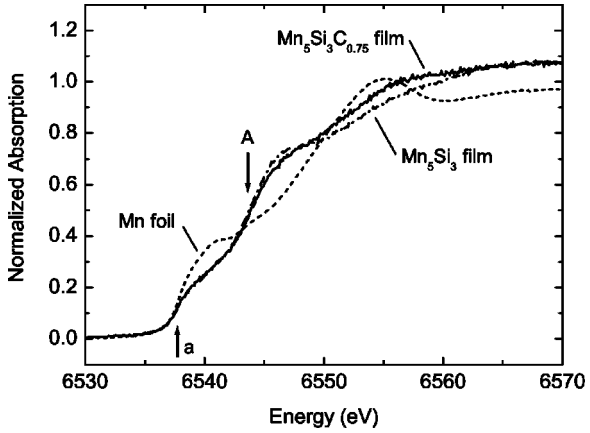

FIG. 8. X-ray-absorption spectra near the Mn K edge of Mn_5Si_3 (dashed-dotted curve) and $Mn_5Si_3C_{0.75}$ (solid curve) films sputtered on sapphire. Dashed curve shows the spectrum of an α-Mn foil for reference. Features labeled a and A indicate the preedge at $E_a = 6537.7$ eV and the main edge at $E_A = 6543.7$ eV for $Mn_5Si_3C_x$ as determined from the inflection points.

also derived from calculations of the partial local densities of electron states.[17] The main absorption edge at *A* is different for the films compared to pure Mn as expected due to the different electronic structure. This edge is caused by transitions from the 1*s* state into the continuum of *p*-like states in the conduction band. However, the important point is that for the $Mn_5Si_3C_x$ films the edge position at $E_A = 6543.7$ eV does not change by carbon incorporation.

In an ionic picture applied to Mn_5Si_3, charge balance requires the presence of four Mn_I^{3+}, six Mn_{II}^{2+}, and six Si^{4-} ions in each unit cell resulting in an average Mn valence of $+2.4$/Mn. The incorporation of C into the voids of the Mn_{II}^{2+} octahedra could induce a charge transfer from Mn_{II} to C, assuming that C is electronegative. This would cause the presence of two Mn_{II}^{2+} and four Mn_{II}^{3+} ions surrounding each C^{-4} ion in $Mn_5Si_3C_x$ and could lead to a double exchange stabilizing ferromagnetic order similar to the colossal magnetoresistance alloys.[2] A change of the average Mn valence from $+2.4$/Mn to $+2.7$/Mn for $x = 0.75$ would give rise to a chemical shift of the absorption edge. XAS on various manganese compounds of different structures and Mn valence have been reported earlier.[17–19] In general, with increasing oxidation state of Mn the *K* edge shifts by about 3–5 eV/valence to higher energies. For the $Mn_5Si_3C_{0.75}$ films an average valence change of 0.3 would shift the Mn *K* edge by 0.9–1.5 eV, which should be easily observable in the spectra. From the fact that such a shift is *not* observed we conclude that a change of the Mn valence by the incorporation of C in $Mn_5Si_3C_x$ films does not occur. This rules out a double exchange to be responsible for the stabilization of ferromagnetic order. Similar reasoning has also been given for $Mn_5Ge_3C_x$ films.[9]

Before turning to the temperature dependence of the EXAFS data we briefly summarize the structural properties of the antiferromagnetic Mn_5Si_3 compound which have been studied intensively by x-ray and neutron diffraction.[22] X-ray diffraction on a single crystal provided evidence that the transition to an antiferromagnetically ordered antiferromagnetic AF2 phase at the Néel point $T_N = 100$ K is accompanied by a small orthorhombic distortion of the hexagonal unit cell normally observed at room temperature. A second magnetic transition to a low-temperature AF1 phase occurs at 66 K which is associated with a change of the *a* and *b* axes and a discontinuity of the *c* axis.[22] These magnetic transitions have also been observed in specific-heat measurements.[23] It is not *a priori* clear whether or not such a structural phase transition takes place in the $Mn_5Si_3C_x$ films. For the present films the investigation of a possible structural phase transition by x-ray diffraction is hampered by the small intensities of the polycrystalline material and by the minor effects of the distortion on a small number of reflections. In this respect, EXAFS measurements can provide additional information about the local atomic order around the absorbing Mn atom.[20]

For this purpose, multiple EXAFS scans were taken at temperatures $T = 5$ K, 82 K, and 150 K in the energy range 6400–7500 eV. The scans were averaged and singular glitches from the monochromator were removed to obtain the fluorescence intensity $I(E)$ prior to further data processing. The normalized intensity $\chi(E)_{exp} = [I(E) - I_0(E)]/[I_0(E) - I_{bac}(E)]$ was obtained by substraction of the preedge background $I_{bac} \propto E$ and normalization to I_0 far above the edge. Figure 9 shows the normalized absorption data of the samples vs photon energy *E*. The energy was converted into the wave vector of the photoelectron by $k(\text{Å}^{-1}) = 0.512\,31\sqrt{E(\text{eV}) - E_0}$ with a threshold energy $E_0 = 6543$ eV. The residual background was approximated by a cubic-spline fit and subtracted to obtain the EXAFS oscillations $\chi_{exp}(k)$. In order to compare the absolute EXAFS signal of the films with the signal of the powder reference sample the correction of self-absorption effects turned out to be important. Eventually, we obtain the true EXAFS oscillation $\chi(k) = \chi_{exp}(k)/(1 - S)$ where *S* depends on the absolute absorption of the fluorescing atoms, the film thickness, the x-ray incidence angle, and the angle between sample and detector.[21] Theoretically, the EXAFS oscillations resulting from all scattering paths *j* from the absorber atom are given by[20,24]

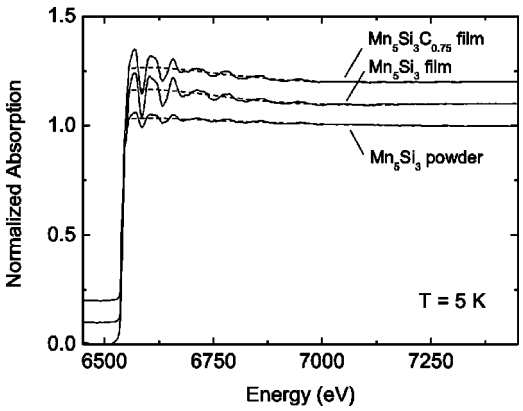

FIG. 9. Normalized x-ray absorption vs photon energy *E* at $T = 5$ K for the investigated samples. Data are successively shifted upward by 0.1 for clarity. Dashed lines show the polynomial splines used to extract the EXAFS oscillations.

$$\chi(k) = \sum_j \frac{N_j S_0^2 F_j}{k R_j^2} \sin(2kR_j + \delta_j) \exp\left(\frac{-2R_j}{\lambda}\right) \times \exp(-2k^2\sigma_j^2), \quad (1)$$

where the presence of higher-order cumulants has been neglected (N, coordination number; S_0^2, amplitude reduction factor; $F(k)$, backscattering amplitude; R, distance; $\delta(k)$, phase; λ, photoelectron mean free path; σ, disorder parameter). The last term in Eq. (1) represents the Debye-Waller factor which takes thermal effects into account.

Figure 10 shows $\chi(k)k^3$ for the three samples at $T = 5$ K. Apart from differences in the range $k > 10$ Å^{-1} the spectra of the films show a similar behavior compared to the powder sample which confirms the presence of the Mn_5Si_3 phase in the films as already deduced from x-ray diffraction. In order to analyze the local atomic order in more detail the EXAFS data were Fourier transformed by application of a

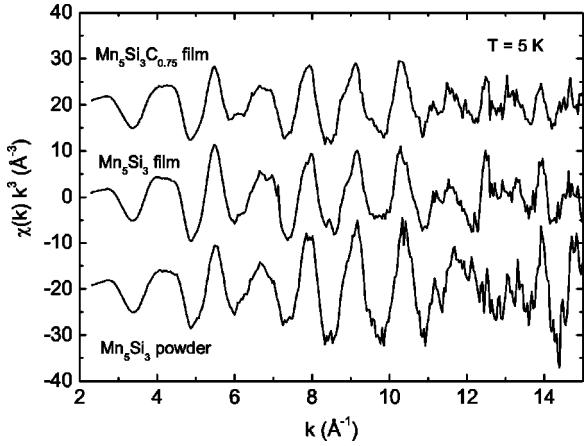

FIG. 10. EXAFS oscillations $\chi(k)k^3$ at $T=5$ K. Data are vertically shifted by 20 Å^{-3} with respect to each other for clarity.

Bessel window. In general, the Fourier transform (FT) allows a separation of the different configuration shells vs distance R from the absorbing atom.

Figure 11 shows the magnitude $|\text{FT}(R)|$ of the $Mn_5Si_3C_x$ samples at various temperatures T. All datasets exhibit a broad peak located at 2–3 Å which arises from the first coordination shells around the Mn_I and Mn_{II} center atoms, followed by smaller peaks due to higher coordination shells. The latter are not due to noise because these peaks remain even after applying various filter procedures on the $\chi(k)k^3$ data before performing the Fourier transform. The data of the Mn_5Si_3 powder reference sample clearly change with decreasing temperature, in particular for a distance R between 3 Å and 4 Å. Moreover, the height of the first-shell peak changes irregularly with T. This is interpreted as being due to the two structural phase transitions occurring at 100 K and 66 K as mentioned above. In contrast, data taken on the $Mn_5Si_3C_x$ films show a very similar behavior for all T which seems to be independent of carbon content, cf. films with $x=0$ and 0.75 in Fig. (11). This strongly suggests that both films do not exhibit an orthorhombic distortion—not even the undoped Mn_5Si_3 film—in contrast to the bulk Mn_5Si_3 powder sample. The lack of such a phase transition in the films could be due to an impeding influence of the sapphire substrate.

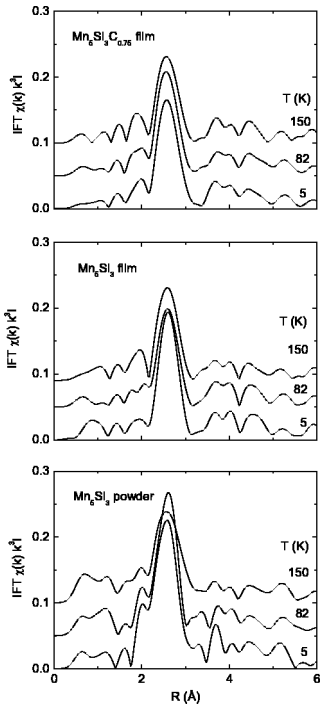

FIG. 11. Fourier transform of the EXAFS oscillations $|\text{FT}\chi(k)k^3|$ vs distance R from the Mn atom of the investigated samples at different temperatures T. In each panel the upper two curves are successively shifted upward by 0.05 for clarity.

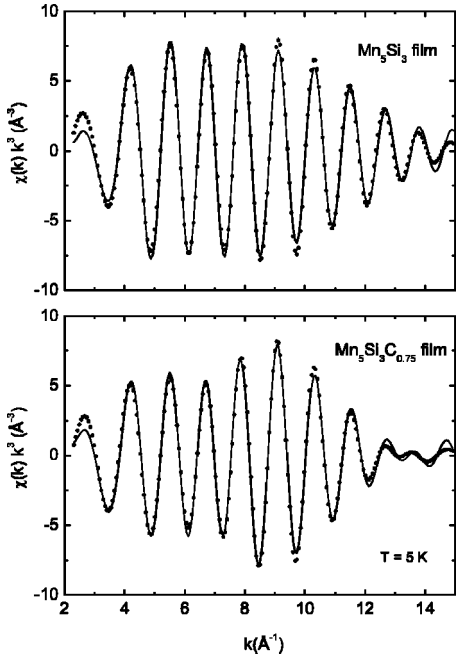

FIG. 12. First-shell filtered data obtained by back transformation of $|\text{FT}(R)|$ (Fig. 11) in the range 1.6 Å$\leqslant R \leqslant$3.2 Å. Dots indicate measured data for $T=5$ K, solid lines are the calculated oscillations using FEFF6 code, see text.

In order to investigate the role of carbon on the local structure in $Mn_5Si_3C_x$ a comparison of the experimental data with a calculation of the EXFAS by an *ab initio* multiple scattering approach would be highly useful.[24] Unfortunately, a reliable result for the whole range of distances up to $R=6$ Å could not be obtained due to the large number of different atom sites and therefore scattering paths which results in a large number of free parameters. However, a calculation was performed by restriction to the first coordination shell, thereby reducing the number of free parameters. For this purpose, first-shell filtered $\chi(k)k^3$ data of the films were obtained by back transformation of $|\text{FT}(R)|$ for the lowest temperature $T=5$ K in the range $R=1.6$–3.2 Å, see Fig. 12. The parameters of the theoretical EXAFS signal obtained from FEFF6 code[25] were refined by application of Eq. (1) to obtain a best fit to the experimental data.[16] Lattice parameters deduced from x-ray-diffraction data taken at $T=25$ K by assuming the hexagonal Mn_5Si_3 structure were used as input parameters.[26] Thermal broadening was taken

TABLE I. Structural data of the first coordination shell obtained by fitting the parameters in Eq. (1) to the experimental EXAFS data for $T=5$ K using scattering paths calculated by FEFF6. Center atoms: Mn_I and Mn_{II} (left part of bond). N, coordination number; d_{XRD}, interatomic distance calculated from the lattice parameters obtained from x-ray diffraction at $T=25$ K; d_{EXAFS}, interatomic distance obtained from the best EXAFS fit. All distances in angstrom.

		Mn_5Si_3 film		$Mn_5Si_3C_{0.75}$ film	
Bond	N	d_{XRD}	d_{EXAFS}	d_{XRD}	d_{EXAFS}
Mn_I-Mn_I	2	2.396	2.40	2.415	2.40
Mn_I-Si	6	2.422	2.44	2.434	2.45
Mn_I-Mn_{II}	6	2.952	2.96	2.967	2.97
Mn_{II}-C	2			2.03	1.91
Mn_{II}-Si	2	2.407	2.36	2.416	2.40
Mn_{II}-Si	1	2.505	2.49	2.516	2.40
Mn_{II}-Si	2	2.653	2.61	2.672	2.81
Mn_{II}-Mn_{II}	2	2.816	2.82	2.878	2.85
Mn_{II}-Mn_{II}	4	2.895	2.89	2.915	2.86
Mn_{II}-Mn_I	4	2.952	2.96	2.966	2.97

into account by application of the correlated Debye model[24] with a Debye temperature $\theta_D=377$ K.[27] The calculation was done by using a weighted set of scattering paths starting at the Mn center atoms at the two different sites of symmetry, i.e., $0.4Mn_I+0.6Mn_{II}$. First, the data of the Mn_5Si_3 film were fitted to obtain the local energy shifts $E_0^{Mn}=2.4$ eV, $E_0^{Si}=0.2$ eV. All coordination numbers were kept fixed and the interatomic distances were refined by correlation to one expansion coefficient. The best fit is plotted in Fig. 12 with interatomic distances d_{EXAFS} given in Table I. These data served as a reference for the fit of the $Mn_5Si_3C_{0.75}$ data, where the E_0 values were taken from the previous fit applied to the Mn_5Si_3 film. However, attempts to obtain a reasonable result by either assuming a linear expansion of the lattice due to the incorporation of carbon, or by taking an additional broadening σ_{dis} due to static disorder into account, or by considering a reasonable change in the coordination numbers were not successful. The best fit plotted in Fig. 12 was obtained by using the interatomic distances as free parameters instead of a correlation to one expansion coefficient. Although the fit in Fig. 12 describes the data well and the interatomic distances around Mn_I are in good agreement with the x-ray data, see Table I, the interatomic distances of the Mn_{II} octahedra show a strongly anisotropic distortion. We emphasize that this result is independent of slight changes of the structural parameter y determining the positions of atoms located at the crystallographic $6(g)$ sites. This is in contrast to the simple picture of a lattice expansion by the incorporation of carbon. An anisotropic distortion of the structure by carbon was also reported for isostructural $Ti_5Si_3C_{0.47}$ compounds which were synthesized by arc melting and structurally characterized by x-ray and neutron diffraction.[28] This result strongly suggests that the carbon is not an ''inert'' interstitial atom but participates in the chemical bonding to Mn. We mention that the fit could not be improved by considering a scenario where the octahedral site was partially occupied by Si.

IV. SUMMARY

The enhanced carbon incorporation in $Mn_5Si_3C_x$ films prepared by magnetron sputtering at elevated substrate temperatures gives rise to magnetic properties, characteristic for a ferromagnet with $T_C=352$ K for $x=0.75$. This is due to an anisotropic modification of the local structure around the Mn sites by carbon, in particular at the octahedral positions, in contrast to the simple picture of an isotropic lattice expansion. In addition, the carbonization seems to have a positive effect on the thermodynamic stability against reaction with a silicon substrate.

We have shown that the formation of the $Mn_5Si_3C_x$ phase takes place in a limited range of substrate temperatures between 300 °C and 500 °C. This is in quantitative agreement with previous reports on Mn/C/Si triple layers[12] and C/Mn/C/Si multilayers.[13] This suggests that the ferromagnetic phase in the latter systems is akin to the ferromagnetic phase in the $Mn_5Si_3C_x$ films investigated here.

ACKNOWLEDGMENTS

We thank M. Hagelstein and E. Dormann for several useful discussions and S. Laurent for performing the resistance measurements. This work was financially supported by the Deutsche Forschungsgemeinschaft.

*Present address: Advanced Photon Source, Argonne National Laboratory, 9700 S. Cass Avenue, Argonne, IL 60439.

[1] C. Pfleiderer, S.R. Julian, and G.G. Lonzarich, Nature (London) **414**, 427 (2001).
[2] R. von Helmolt, J. Wecker, B. Holzapfel, L. Schultz, and K. Samwer, Phys. Rev. Lett. **71**, 2331 (1993).
[3] J.P. Sénateur, J.-P. Bouchaud, and R. Fruchart, Bull. Soc. Fr. Mineral. Cristallogr. **90**, 537 (1967).
[4] *International Tables of Crystallography*, edited by T. Hahn (Reidel, Dordrecht, 1983), Vol. A.
[5] E. Parthé, W. Jeitschko, and V. Sadagopan, Acta Crystallogr. **19**, 1031 (1965).
[6] J.D. Corbett, E. Garcia, A.M. Guloy, W.-M. Hurng, Y.-U. Kwon, and E.A. Leon-Escamilla, Chem. Mater. **10**, 2824 (1998).
[7] M. Gajdzik, C. Sürgers, M. Kelemen, and H.v. Löhneysen, J. Appl. Phys. **87**, 6013 (2000).
[8] M. Gajdzik, C. Sürgers, M. Kelemen, B. Hillebrands, and H.v. Löhneysen, Appl. Phys. Lett. **68**, 3189 (1996).
[9] M. Gajdzik, C. Sürgers, M. Kelemen, and H.v. Löhneysen, J. Magn. Magn. Mater. **221**, 248 (2000).
[10] M.T. Kelemen, M. Gajdzik, C. Sürgers, H.v. Löhneysen, and E. Dormann, Phys. Lett. A **269**, 234 (2000).
[11] C. Sürgers, H.v. Löhneysen, M.T. Kelemen, E. Dormann, and M.S.S. Brooks, J. Magn. Magn. Mater. **240**, 383 (2002).
[12] T. Takeuchi, M. Igarashi, Y. Hirayama, and M. Futamato, J. Appl. Phys. **78**, 2132 (1995).

[13] R. Nakatani, T. Kusano, H. Yakame, and M. Yamamoto, Jpn. J. Appl. Phys., Part 1 **41**, 5978 (2002).
[14] M. Gajdzik, Ph.D. thesis, Universität Karlsruhe, 1999.
[15] *Practical Surface Analysis*, edited by D. Briggs and M. P. Seah (Wiley, New York, 1990), Vol. 1.
[16] T. Ressler, J. Phys. IV **7**, C2 (1997), see also http://www.winxas.de for further information.
[17] R. Nietubyć, E. Sobczak, and K.E. Attenkofer, J. Alloys Compd. **328**, 126 (2001).
[18] S.I. Salem, C.N. Chang, P.L. Lee, and V. Severson, J. Phys. C: Solid State Phys. **11**, 4085 (1978).
[19] M.Y. Apte and C. Mande, J. Phys. C **15**, 607 (1982).
[20] *X-Ray Absorption: Principles, Applications, Techniques of EXAFS, SEXAFS, and XANES*, edited by D. C. Koningsberger and R. Prins (Wiley, New York, 1988).
[21] R. Castañer and C. Prieto, J. Phys. III **7**, 337 (1997).
[22] P.J. Brown and J.B. Forsyth, J. Phys.: Condens. Matter **7**, 7619 (1995), and references therein.
[23] N.P. Sudakova, S.I. Kuznetsov, A.V. Mikhel'son, N.I. Sychev, and N.V. Gel'd, Dokl. Akad. Nauk SSSR **228**, 582 (1976) [Sov. Phys. Dokl. **21**, 273 (1976)].
[24] J.J. Rehr and R.C. Albers, Rev. Mod. Phys. **72**, 621 (2000), and references therein.
[25] J.J. Rehr, R.C. Albers, and S.I. Zabinsky, Phys. Rev. Lett. **69**, 3397 (1992).
[26] The FEFF input file containing the atomic positions was generated by the program ''Atoms'' written by B. Ravel which can be used via the internet under http://millenia.cars.aps.anl.gov/cgi-bin/atoms/atoms.cgi
[27] G.I. Kalishevich, N.P. Sudakova, A.V. Mikhel'son, N.V. Gel'd, and V. I Surikov, Sov. Phys. Solid State **16**, 1386 (1975).
[28] J.J. Williams, M.J. Kramer, M. Akinc, and S.K. Malik, J. Mater. Res. **15**, 1773 (2000).